Journal of Magnetic Resonance **156,** 131–137 (2002)
doi:10.1006/jmre.2002.2548

Optimizing STMAS

Clarisse Huguenard,* Francis Taulelle,*,[1] Benno Knott,† and Zhehong Gan‡,[1]

*RMN et Chimie du Solide, FRE 2423 Tectonique Moléculaire du Solide ULP-CNRS, University Louis Pasteur, 4 Rue Blaise Pascal, 67070 Strasbourg Cedex, France; †Bruker Analytik GmbH, Silberstreifen, 76287 Rheinstetten, Germany; and ‡Center of Interdisciplinary Magnetic Resonance (CIMAR), National High Magnetic Field Laboratory (NHMFL), 1800 East Paul Dirac Drive, Tallahassee, Florida 32310

Received December 17, 2001; revised April 12, 2002

The 2D satellite transition magic angle spinning (STMAS) experiment generates efficiently high-resolution isotropic NMR spectra of half-integer quadrupolar nuclei. The experiment involves excitation and coherence transfer of satellite transitions into the central transition. It requires efficient refocusing of satellite transitions and sample spinning at a very accurate magic angle to cancel the first-order quadrupolar interaction effect. A review of all parameters relevant to optimizing the STMAS experiment is presented, including pulse sequence calibration, regulating spinning speed, magic angle adjustment, optimization of satellite transition excitation, and coherence transfer for both $I = 3/2$ and $I \geq 5/2$ nuclei.

Key Words: **quadrupolar nuclei; satellite transition magic angle spinning (STMAS); magic angle calibration; second-order quadrupolar effect.**

INTRODUCTION

The 2D satellite transition magic angle spinning (STMAS) experiment correlates satellite and central NMR transitions of half-integer quadrupolar nuclei under magic angle spinning (MAS). The correlation can generate coherence-transfer echoes leading to isotropic NMR spectra (*1, 2*) with the assumption that the first-order quadrupolar interaction is completely averaged. The average of the large first-order quadrupolar interaction requires precise experimental settings. Some of the requirements are so rigid that several groups have experienced difficulties in setting up the experiment successfully, raising the issues of optimizing STMAS.

The STMAS experiment follows the general scheme of 2D NMR experiments: excitation, evolution, mixing, and acquisition. During the evolution period, the first-order quadrupolar interaction to satellite transitions (ST) must be averaged in order to generate isotropic NMR spectra. The average relies on the refocusing of ST by MAS. Because quadrupolar interactions are typically on the order of MHz, ST rotational echoes are extremely sharp and sensitive to the setting of a magic angle. Thus, small errors on synchronization of evolution time t_1 with rotational echoes and on magic angle setting can lead to severe degradation of the performances. Furthermore, CT–CT and ST–ST auto-correlation peaks appear along the diagonal of 2D single-quantum spectra. These unwanted peaks contain no additional spectral information but hinder the readability of the ST–CT peaks. Suppression of diagonal peaks, especially the strong CT–CT peaks, is desired. In this paper, magic angle setting, pulse sequence timing, spinning speed stability, diagonal peak suppression, and other experimental aspects of the STMAS experiment are described for optimizing STMAS using test samples for both $I = 3/2$ and $I = 5/2$ spins.

[1] To whom correspondence should be addressed. E-mail: taulelle@chimie.u-strasbg.fr, gan@magnet.fsu.edu.

EXPERIMENTAL

Sodium sulfate and $AlPO_4$ berlinite are selected as model compounds for optimizing a STMAS of $I = 3/2$ and $I = 5/2$ nuclei. Both samples are commercially available or can be synthesized easily (*3*) and exhibit a single site with good spectral sensitivities. The samples have the following NMR parameters: for $^{23}Na_2SO_4$, $\delta_{iso} = -8.7$ ppm relative to solid NaCl or a saturated solution in water, $C_Q = 2.560$ MHz, and $\eta_Q = 0.6$; for $^{27}AlPO_4$, $\delta_{iso} = 42.7$ ppm relative to $Al(H_2O)_6^{3+}[3(NO)_3^-]$ in water solution, $C_Q = 4.067$ MHz, and $\eta_Q = 0.35$.

The optimizing procedure was carried out on a Bruker DSX 500-MHz spectrometer using a 4-mm MAS probe. A standard pneumatic unit from Bruker was used for regulating the MAS spinning speed at 12500 Hz. The RF field is $\omega_1/2\pi = 50$ kHz for hard pulses and 5 kHz for soft pulses. The repetition delay was 0.5 s and 32 dummy scans were used for calibration with 1D experiments.

Pulse Sequences for STMAS

Variation of ST–CT coherence transfer can lead to three types of STMAS sequence in full analogy with the MQMAS experiment which correlates MQ and CT (*4, 5*) (Fig. 1). The two-pulse sequence uses a single mixing pulse for the ST–CT coherence transfer (Fig. 1a) and acquires 2D data in phase-modulated form (*1, 2*). The coherence transfer pathway generates echoes for $I = 3/2$ spins yielding ridge-shaped peaks with mixed phase. Two types of three-pulse sequences are considered: the first one

1090-7807/02 $35.00

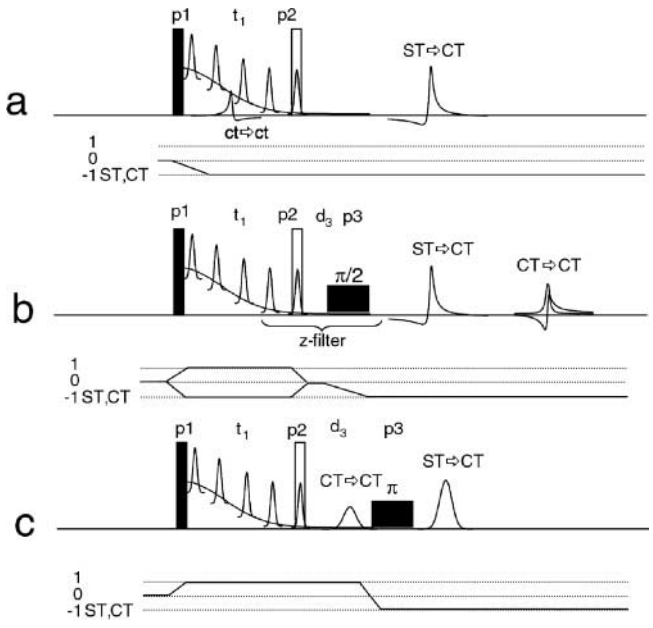

FIG. 1. Pulse sequences and coherence transfer pathway for STMAS experiment with (a) two pulses, (b) z-filter, and (c) echo version of three-pulse sequences. As t_1 increments, ST–CT and CT–CT echoes travel in opposite directions for $I = 3/2$ and the same direction for $I = 5/2$. For $^{23}Na_2SO_4$ ($I = 3/2$), the parameters were $p_1 = 1.75\ \mu s$, $t_1(0) = 78.125\ \mu s$, and $p_2 = 2\ \mu s$ with phase cycle $p_1 = +x, -x$; $p_2 = +x, +x, +y, +y$, and receiver $+x, -x$ for the two-pulse experiment. The parameters for the z-filter three-pulse experiment were $p_1 = 1.75\ \mu s$, $t_1(0) = 78.25\ \mu s$, $p_2 = 1.75\ \mu s$, $d_3 = 40\ \mu s$, and $p_3 = 25\ \mu s$ with phase cycle $p_1 = +x, -x$; $p_2 = +x$ (real), $-y$ (imaginary), $p_3 = +x, +x, -x, -x$, and receiver $+x, -x, -x, +x$. For $^{27}AlPO_4$ berlinite ($I = 5/2$), the parameters were $p_1 = 1.75\ \mu s$, $t_1(0) = 78.125\ \mu s$ and $p_2 = 2\ \mu s$ with phase cycle $p_1 = +x, -x$; $p_2 = +x, +x, +y, +y$, and receiver $+x, -x\ -x, +x$; for the two-pulse experiment. The parameters for the z-filter experiment were $p_1 = 1.5\ \mu s$, $t_1(0) = 78.75\ \mu s$, $p_2 = 1\ \mu s$, $d_3 = 40\ \mu s$, and $p_3 = 16\ \mu s$ with a phase cycle identical to $I = 3/2$.

uses a z-filter between the pair of mixing pulses to acquire the data in hypercomplex form. Amplitude-modulated data yield purely phased lineshape regardless of spin number (*1, 6*). The second type of the three-pulse version adds a π-pulse to the two-pulse sequence. The π-pulse inverts the sign of coherence order, leading to coherence transfer echoes for $I > 3/2$ spins. By increasing the delay before the π-pulse, coherence transfer echoes can be shifted, reducing the twisted lineshape of phase-modulated data. Pure absorptive 2D spectra can be obtained if full coherence transfer echoes are acquired (*7, 8*).

All three sequences have one common feature: the correlation spectra need to be sheared to get a full separation of the isotropic and anisotropic dimensions similar to the MQMAS experiment (*4, 9*). The amount of shearing is determined by the ratio of the fourth rank expansion coefficients between ST and CT, $-9/8$ for $I = 3/2$ and $7/24$ for $I = 5/2$ (*1, 2*). A split-t_1 version of the experiment is possible for samples with long T_2 where the need for shearing can be avoided (*7, 10*). On the choices of the pulse sequences, the simplest two-pulse sequence can be used for optimization. For better lineshape, one can choose the three-pulse version with the z-filtered or the shifted-echo sequence (Figs. 1b and 1c). For samples with short T_2, such as many microporous compounds, the z-filter version is preferred. For samples with long T_2, such as most mineral compounds, one may choose the shifted-echo version to increase the signal-to-noise ratio.

Setting a t_1 Increment, Its First Value, and Spinning Speed Stability

Satellite transition signals dephase rapidly due to the large first-order quadrupolar interaction. Under MAS, ST signals are refocused into rotational echoes generating manifolds of spinning sidebands (Fig. 2). Short dwell time (wide spectral window) is required to digitize sharp rotational echoes. The sideband intensities follow the static powder patterns of the first-order interaction attenuated by limited excitation bandwidth. Assuming a perfect magic angle setting, the echo amplitudes evolve with the second-order quadrupolar interaction in full analogy with CT or 3Q transitions that have zero first-order effect. In the frequency domain, one can describe the rotor synchronous sampling of echo amplitude as a folding of all ST spinning sidebands resulting in a lineshape solely from the second-order quadrupolar effect. For $I = 3/2$, the second-order quadrupolar effect is nearly the same, $|-9/8|$, for ST and CT transitions. For $I = 5/2$ nuclei, the second-order effect to the inner ST pair (ST_1) is more than three times, $24/7$, smaller than CT (*1, 2*).

In order to generate isotropic spectra, ST–CT coherence transfer must occur at the top of rotational echoes where the ST coherences are refocused. The evolution time t_1 must be incremented with the rotor period and the first increment needs to be precisely at $t_1 = \tau_r - (p_1 + p_2)/2$ including the consideration of finite length for excitation (p_1) and mixing (p_2) pulses. The width of rotational echoes (δt_1) is approximately the inverse of ν_Q. For 1-MHz ν_Q, the timing of the mixing pulse must be set within 1 μs.

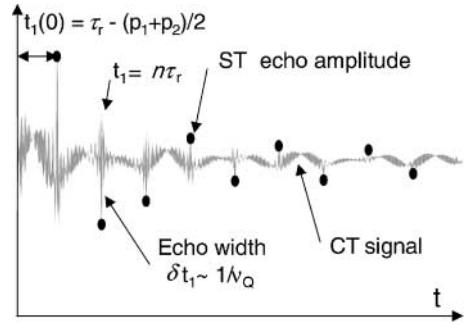

FIG. 2. ST and CT free-induction-decay of $^{23}Na_2SO_4$ under MAS plotted with interleaved real and imaginary points of the time-domain signal. Sharp rotational echoes indicate that synchronous t_1 timing with rotor period is essential for STMAS experiment. ST echo amplitudes and CT signals dephase by the second-order quadrupolar interaction.

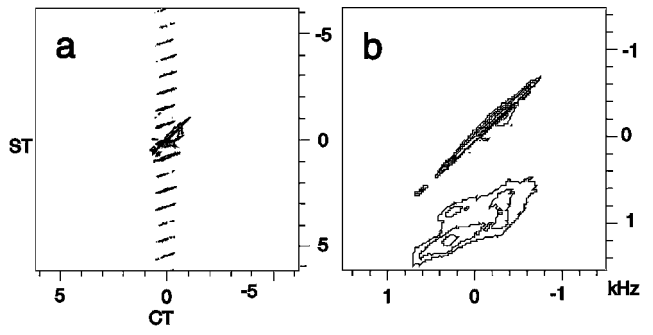

FIG. 3. $^{27}AlPO_4$ berlinite STMAS spectra with spinning frequency (a) 735 Hz and (b) 10 Hz off from synchronous condition. The spectra were acquired using the two-pulse sequence with t_1 increment 85 $\mu s = \tau_r + 5$ μs and (b) 80.065 $\mu s = \tau_r + 0.065$ μs. In (a), the ST–CT correlation is dispersed into $80/5 = 16$ echoes (16 sidebands in the frequency domain). In (b) the slight deviation from synchronous condition leads to broadening the ST–CT peak.

The strict t_1 matching condition makes stable sample spinning essential to the STMAS experiment. A small drift on spinning speed $\Delta\nu_r$ can cause a mismatch $t_1\,\Delta\nu_r/\nu_r$. For the last t_1 increment (typically $t_1 = n\tau_r$ is on the order of T_2^*) the mismatch $T_2^*\Delta\nu_r/\nu_r$ should be smaller than δt_1. Thus, the requirement on spinning frequency stability can be estimated as $\Delta\nu_r/\nu_r < \delta t_1/n\tau_r$. For typical values of $\nu_r \approx 10$ kHz, 32 t_1 points ($T_2^* \approx 3$ ms), and $\delta t_1 \approx 1$ μs, the experiment requires $10{,}000 \pm 3$ Hz stability. For most modern MAS probes and pneumatic units, such stability can be easily fulfilled. At some places, improvement on pressure stability may be necessary and buffering air supplies with a ~100-L tank can be a cheap but viable solution to air pressure fluctuations.

Any imperfection on spinning stability, drift, or fluctuations will produce a convolution of ST echo amplitudes and consequently lead to modulation or broadening along the indirect dimension of the 2D spectra. Figure 3a displays a 2D STMAS spectrum with a t_1 increment deliberately set 1/16th off the synchronous condition. The spectrum shows an apparent oscillation of $\nu_r/\Delta\nu_r = 16$ spinning sidebands in F1. Figure 3 also shows that a small deviation from the required spinning speed broadens the ST–CT peaks.

Suppression of the CT–CT Correlation

Diagonal peaks often obscure the readability of 2D spectra. For small quadrupolar couplings, ST–CT peaks are very close to the diagonal of STMAS spectra, making suppression of diagonal peaks desirable. It is possible to suppress CT–CT diagonal peaks in two ways. In the first option, CT is selectively presaturated by a soft pulse prior to a two- or three-pulse sequence (Fig. 4a). Large differences on spectral width between CT and ST allow a selective suppression of CT peaks without much effect on satellite transitions.

The nutation of central transition peaks under RF irradiation consists of multiple frequency components and does not follow a simple sinusoidal curve as in the case of $I = 1/2$ (*11, 13–16*). It is then necessary to perform an optimization on the sample itself. A simple sequence consisting of a selective soft pulse followed by a delay and a short excitation pulse can be used for optimizing presaturation. Once the RF power of the selective pulse is set, two parameters control optimal CT suppression: the pulse length and the delay before the hard excitation pulse during which magnetization dephases. The selective pulse length is carefully calibrated for optimal suppression of CT and minimal distortion of ST spinning sidebands (Fig. 5a). The interpulse delay can be further fine-tuned for better CT suppression if necessary. For the selected test samples, the CT peaks can be reduced below the height of individual ST spinning sidebands. After the last stage of p_1 and p_2 optimization, the presaturation pulse length may be reoptimized again for the best results.

Figure 5 also shows an additional advantage of CT presaturation: an increase of ST polarization. The first pair of ST shares energy levels with CT; therefore, equalizing polarization by CT presaturation increases ST polarization by 50%. The gain in Fig. 5 is less than the ideal 50% primarily due to the large flip angle for the excitation and the effect from CT presaturation to ST modulated by MAS.

The second method for suppressing CT–CT peaks takes advantage of the sharp ST rotational echoes. By slightly shifting the first t_1 but keeping the same increment, the mixing pulse acts on dephased ST amplitude while the CT signal is nearly unchanged. By subtracting two acquisitions for each t_1 (alternation between a synchronized and a desynchronized scan as shown in Fig. 4b), a 2D STMAS spectrum free of CT–CT peaks can be obtained. This method has the advantage that CT–CT peaks can be subtracted out cleanly without the need for optimization but with a loss of a factor of 2 in signal-to-noise. Figure 6 shows a comparison between the two methods for the sample of $^{27}AlPO_4$

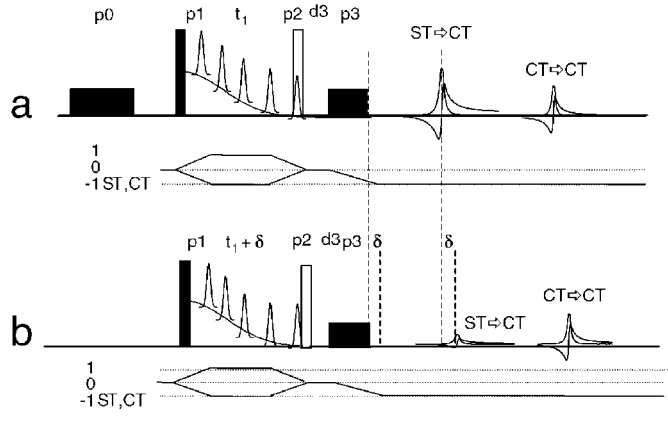

FIG. 4. STMAS sequences that suppress CT–CT diagonal peaks (a) using a soft presaturation pulse and (b) using the subtraction method. In (b), the receiver phase is alternated between synchronized ($\delta = 0$) and desynchronized ($\delta \approx 1$ μs) for subtracting out CT–CT signals. The data acquisition is delayed by δ in order to have identical CT–CT echoes between synchronized and desynchronized experiments at the same time position.

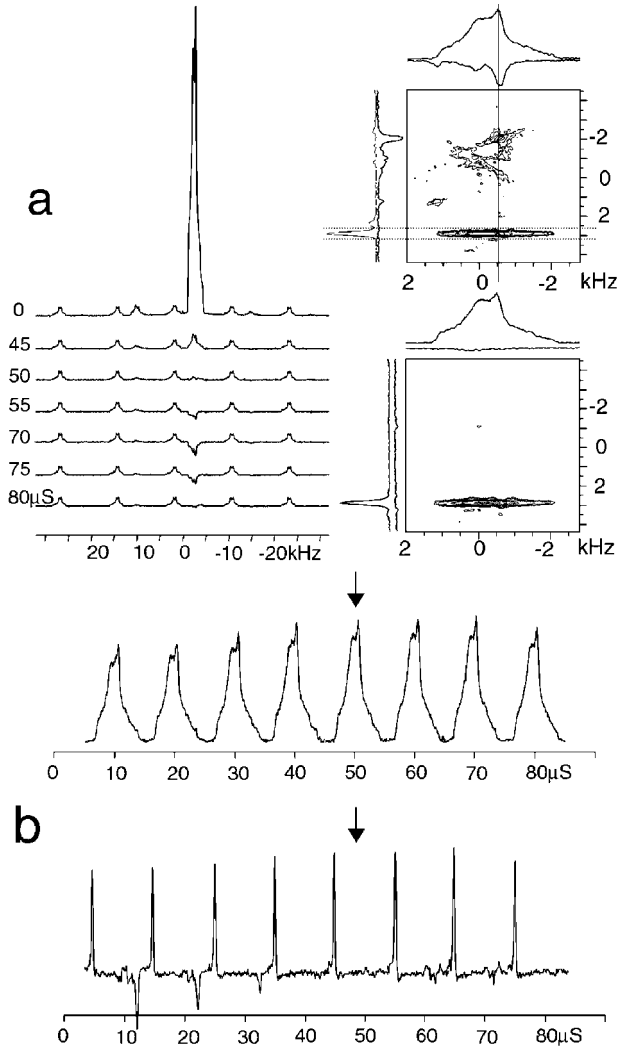

FIG. 5. (a) Pulse length optimization for CT presaturation and comparison between 2D STMAS spectra of $^{23}Na_2SO_4$ without (top) and with (bottom) CT presaturation. (b) Slices of 2D STMAS spectra demonstrating the reduction of the CT–CT diagonal peaks and the increase of the ST–CT peak from CT presaturation (bottom) along the isotropic dimension and (top) along the anisotropic dimension. In the 2D experiments, the hard pulses are $p_1 = 1.75\ \mu$s and $p_2 = 2\ \mu$s, respectively, for the excitation and the mixing. On both axes 0 Hz refers to the position of the carrier. RF field for the soft pulse is $\omega_1/2\pi = 5$ kHz and optimal presaturation is obtained with $p_0 = 50\ \mu$s and a 50-ms delay before the excitation.

berlinite. Suppression of CT–CT by presaturation is not complete here, while the subtraction method removes the CT–CT ridge almost perfectly.

Magic Angle Setting

Magic angle calibration is the most important factor in the STMAS experiment. Under fast MAS, ST spinning sidebands can be readily observed with wide spectral windows and short excitation pulses (*14, 16–19*). Through minimizing the width of spinning sidebands or maximizing the rotational echo amplitude, the magic angle can be calibrated within an accuracy of a few tenths of a degree using samples with small quadrupolar couplings such as $K^{79}Br$, $^{23}NaNO_3$, and $Y_3^{27}Al_5O_{12}$ (*17, 18*). Figures 7 and 8 show the change of ST spinning sideband intensities, lineshape, and STMAS spectra of $^{23}Na_2SO_4$ and $^{27}AlPO_4$ berlinite for five different angle settings from bad (*1*) to good (*5*). The sideband intensities show nearly no difference from (*3*) to (*5*), which indicates limited accuracies. The second-order quadrupolar interaction interferes with the residual first-order quadrupolar interactions scaled by $P_4(\cos\theta_S)$, which makes the adjustment insensitive.

A careful inspection of ST sideband lineshape can reveal the change of angle setting from (*3*) to (*5*). Assuming a perfect magic angle setting, the ST peaks should have the same lineshape with CT. For $I = 3/2$, the ratio between ST and CT is $-9/8$, which suggests a reversed shape with similar width (*14, 16, 18, 19*). The ratio for $I = 5/2$ is $7/24$; thus, the ST peaks should be more than three times narrower than CT (Fig. 8b). It should be generally recommended to use $I = 5/2$ spins for magic angle setting because of the long-lasting ST echoes compared to CT. In the MAS spectra of berlinite (Fig. 8c), one can notice an unusual feature in the left side of the CT peak. The separation of the ST centerband (ST_1 # 0) from the CT peak is a net function of the angle setting. The separation could be used for an easy check of magic angle setting from the 1D ^{27}Al MAS spectra of berlinite.

The most accurate magic angle calibration is by the 2D STMAS experiment itself. High efficiencies of the STMAS experiment allow rapid acquisition of the 2D spectra of the test compounds. The effects of angle setting on STMAS are depicted in Figs. 7c and 8d. A small deviation from the magic angle reintroduces a residual first-order quadrupolar interaction in the t_1 evolution. The splitting along the indirect dimension is

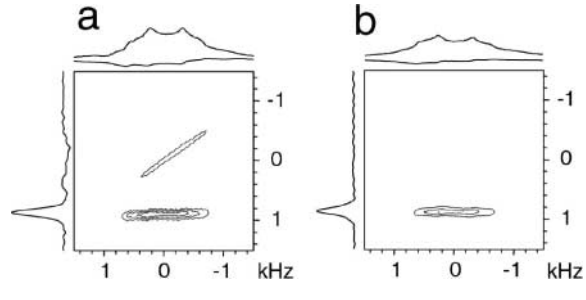

FIG. 6. $^{27}AlPO_4$ berlinite STMAS spectra demonstrating CT subtraction. The spectrum in (a) was acquired using a soft CT presaturation pulse with the two-pulse sequence. Eight scans and 256 fids were collected in 18 min. Residual CT–CT peaks as shown in the negative sum projection are due to incomplete CT presaturation. The spectrum in (b) was acquired using the subtraction method described in the text. The desynchronizing delay was 2 μs. The phase cycle was doubled and receiver phase was modified to perform the desired subtraction: $p_1 = +x, +x, -x, -x$; $p_2 = +x, +x, +x, +x, +y, +y, +y, +y$, receiver $+x, -x, -x, +x, -x, +x, +x, -x$. 16 scans and 256 fids were collected in 36 min. Both spectra were phased such that the ST–CT peak is positive and 0 Hz refers to the position of the carrier along both axes.

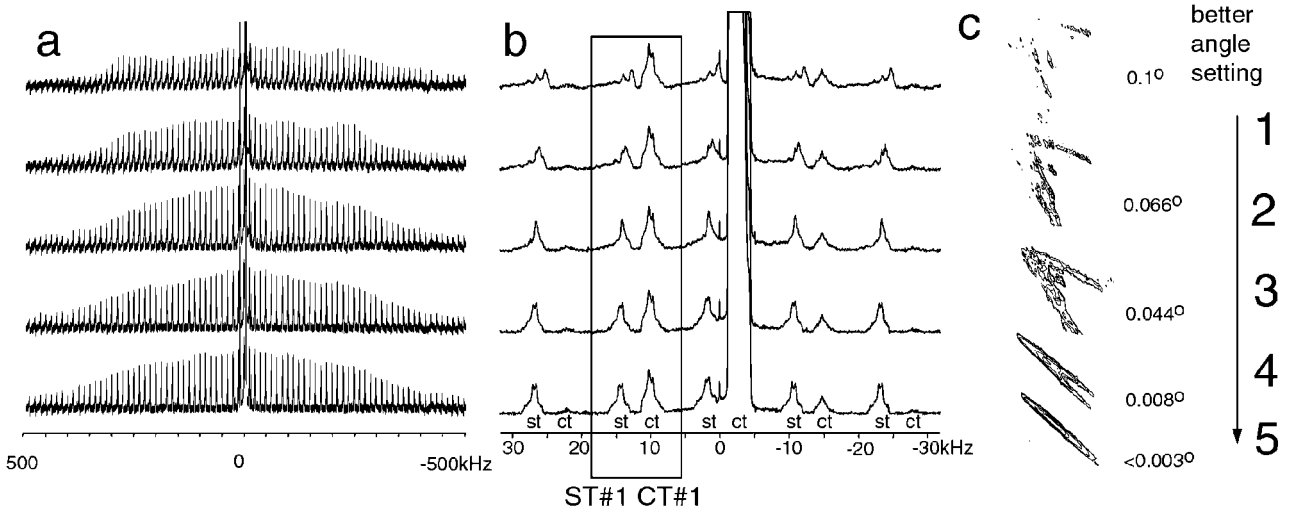

FIG. 7. ^{23}Na MAS and STMAS spectra of Na_2SO_4 for magic angle calibration. (a) MAS spectra in full view with 1-MHz spectral width, (b) zoomed spectra showing sideband lineshape, and (c) 2D STMAS spectra from bad (1) to good (5) magic angle setting as displayed. The details of the experiments were described in the text and Fig. 1. The nonsheared 2D STMAS spectra were acquired using the two-pulse sequence with a soft pulse for CT suppression.

given by the static first-order quadrupolar interaction scaled by $P_2(\cos\theta_S)$:

$$\Delta\nu_{F_1} = 2\nu_Q P_2(\cos\theta_S). \quad [1]$$

The deviation from the magic angle can therefore be estimated from the splitting $\Delta\nu_{F_1}$ F_1 along (2):

$$\Delta\theta_M = \frac{\sqrt{2}\Delta\nu_{F_1}}{4\nu_Q}. \quad [2]$$

Because the STMAS experiment refocuses the second-order quadrupolar interaction, the magic angle can be calibrated with high accuracies by monitoring the scaling to the first-order quadrupolar interaction without interference from the second-order terms.

Monitoring ST–CT echoes can be helpful in both magic angle adjustment and pulse length calibration. The ratio of the fourth rank expansion coefficients between ST and CT is negative, $-9/8$, for $I = 3/2$ and positive, $7/24$, for $I = 5/2$. ST–CT and CT–CT echoes appear at different positions in FID (Fig. 9). For $I = 3/2$ if one follows a $(0, -1, -1)$ coherence pathway, ST–CT coherence transfer is an echo, $t_2 = -(-8/9)t_1$, while the CT–CT signal is an antiecho, $t_2 = -t_1$. When increasing t_1,

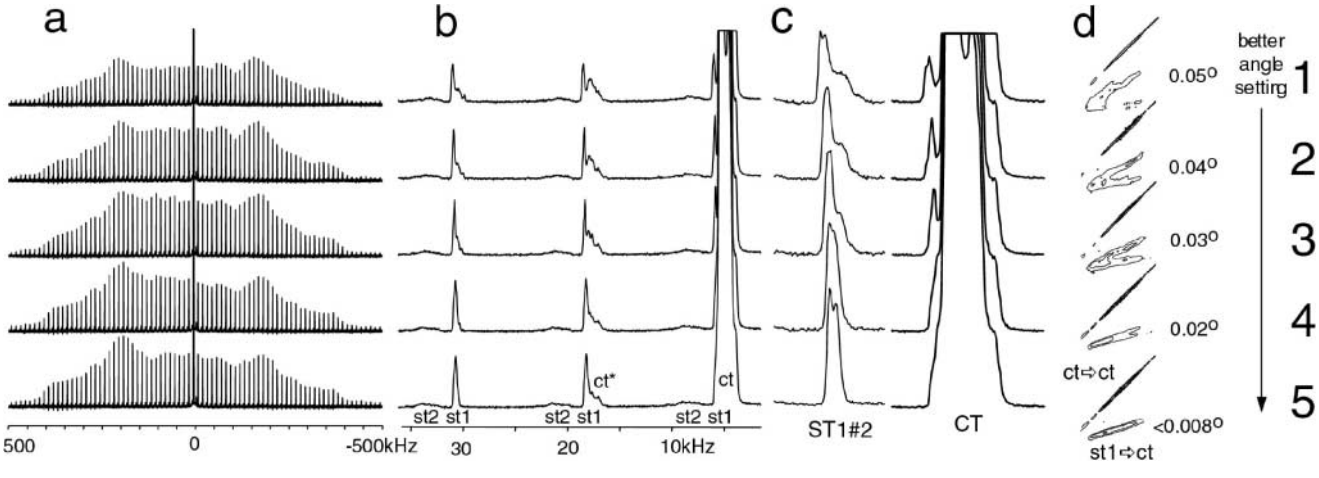

FIG. 8. ^{27}Al MAS and STMAS spectra of $AlPO_4$ berlinite for magic angle calibration. (a) MAS spectra in full view with 1-MHz spectral width, (b) zoomed spectra showing sideband lineshape of the first (st1) and the second (st2) pairs of satellite transitions, (c) spectral features that are sensitive to the magic angle setting, and (d) 2D STMAS spectra from bad (1) to good (5) magic angle setting as displayed. The details of the experiments were described in the text and Fig. 1. The nonsheared 2D STMAS spectra were acquired using the two-pulse sequence with a soft pulse for CT suppression. The remaining diagonal peak is due to incomplete CT presaturation.

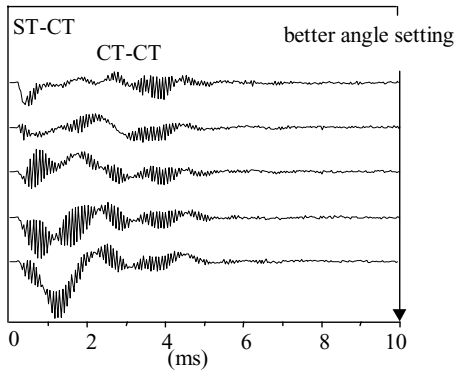

FIG. 9. Magic angle adjustments by monitoring ST–CT coherence transfer echoes. The ^{27}Al FIDs of $AlPO_4$ berlinite were acquired with the 1D version of the two-pulse STMAS sequence and the echoes are plotted with interleaved real and imaginary points. A long evolution time, $t_1 = 3198.125$ μs (40th fid of a 2D experiment), was selected such that ST–CT and CT–CT echoes are well separated as indicated in the figure. Other parameters are described in Fig. 1. The magic angle can be calibrated by maximizing the ST–CT echo.

the CT–CT signal shifts backward and the ST–CT signal moves forward along t_2. For $I = 5/2$ with a $(0, +1, -1)$ coherence transfer pathway, both ST–CT and CT–CT signals appear as echoes. The echo positions are different between ST–CT, $t_2 = (7/24)t_1$, and CT–CT, $t_2 = t_1$, and they appear separated after a long t_1. For all $I > 5/2$ spins, the ST–CT echo behavior is similar to $I = 5/2$ spin because of the positive sign for the expansion coefficient ratios (*2*).

While magic angle tuning has little effect on the CT–CT signal, it has a dramatic effect on ST–CT echoes. The time-domain data for a particular t_1 consist of two superimposed echoes, one from ST^+ $(3/2 \rightarrow 1/2)$ and the other from ST^- $(-1/2 \rightarrow -3/2)$. The residual first-order quadrupolar interaction scaled by $P_2(\cos\theta_S)$ has different signs to ST^+ and ST^-. When the spinning axis is slightly off the magic angle, ST^+–CT and ST^-–CT echoes are shifting away from each other. At the same time, the echo amplitude is attenuated by the residual first-order interaction. The magic angle can therefore be finely adjusted by monitoring the amplitude of the overall ST–CT echo as shown in Fig. 9. Such a calibration carried out with a 1D experiment can be monitored in real-time for test samples with good sensitivities.

Optimization Strategy

The actual sequence to set an STMAS experiment may not follow the order of discussion given above. A recommended sequence of steps to perform an STMAS experiment is therefore given below.

Before the experiment, the probe should be tightly mounted to the magnet so that sample change (if equipped with an automatic sample changer), probe tuning, and angle adjustment would not disturb the probe orientation. A careful check of spinning stability (or improvement if greater than 2 Hz) must be done. The magic angle should be set as accurately as possible using the conventional method, typically within a tenth of a degree.

First, satellite transition signals should be observed directly using a wide spectral window (~1 MHz) and a hard excitation pulse (<1 μs). The spectra can be acquired rapidly as ST transitions are unlikely to be saturated by small tip angle pulses. For $I = 3/2$ spins, a comparison between CT and ST lineshapes can be used to monitor the magic angle setting. For $I = 5/2$ spins, narrow ST peaks over CT are expected when the magic angle is set. The position of the ST centerband indicates the ST peak position along the indirect dimension for the 2D spectra later.

Calibration of CT presaturation uses a soft pulse followed by a delay before the hard excitation pulse as described in Fig. 5. Both pulse and delay must be optimized to reduce the strong CT peak to a level comparable to ST spinning sidebands and the distortion from the soft pulse to ST sidebands should be kept minimal. As these values are not totally independent of the following pulses, a later reoptimization should be undertaken when finished with the other steps. No special optimization is required for suppression of CT–CT by desynchronization-subtraction.

Usually the simplest two-pulse sequence allows for optimizing the magic angle, p_1, p_2. The starting t_1 must be set to $\tau_r - (p_1 + p_2)/2$ with a t_1 time increment matching exactly one rotor period. A calibration on t_1 could give a sense of the extreme sensitivity on t_1 timing of the STMAS experiment. Nevertheless, this calibration may not be necessary as it can be predicted by $\tau_r - (p_1 + p_2)/2$. The minimum t_1 is used for minimizing the losses due to magnetization decay and other complications such as magic angle setting, but is long enough to separate ST–CT echo from CT–CT. It should be remembered that the optimal pulse length not only depends on RF field strength but also on the magnitude of quadrupolar interactions (*11*). Harder pulses cover a wider spectral window for samples with large quadrupolar coupling constants. The sensitivity of STMAS increases with a more effective excitation of satellite transitions (*12*). However, for the test samples considered, STMAS works quite well with a moderate RF field of 50–80 kHz. The excitation p_1 and mixing p_2 pulse lengths can be set to about 1 μs for typical RF field strength $\omega_1/2\pi$ around 50~80 kHz. With the observation of the ST–CT echo, both p_1 and p_2 are optimized iteratively by rechecking that p_1 is optimum after optimization of p_2.

Two methods can be used to calibrate the magic angle: maximizing ST–CT echo or rapid acquisition of the 2D STMAS spectra of test samples. When using the echo method, 10 to 50 rotor cycles for t_1 allow separation of ST–CT from CT–CT (Fig. 9). Eventually, the angle setting should be checked by running a 2D STMAS experiment. A sharp ridge-shaped peak is expected when the magic angle is precisely set. A small deviation of the angle setting would split the peak and the angle offset could be estimated using Eq. [2].

For coarse and jumpy wind for adjusting the magic angle, several attempts may be required to find an angle accurate enough for STMAS experiments. The angle adjustment may also encounter difficulties for MAS stators that are worn out by frequent

landings of fast spinning rotors. During angle adjustment, the coherence transfer echo may disappear due to over-turning the spinning axis. In this case, the spinning axis can be returned to the magic angle approximately by observing rotational echoes from the single pulse experiment. Probes with a smooth angle control and fine mechanical thread help considerably in setting and keeping the angle exactly at the magic angle.

The choice of pulse sequence to reduce a phase-twisted lineshape can be made based on the sample's T_2. For a z-filter sequence (short T_2), the delay between p_2 and p_3 is chosen to be short, usually one rotation period, and p_3 is a selective 90° pulse with low RF power. The pulse length p_3 eventually is optimized on an echo amplitude as p_1 and p_2. For a shifted echo sequence (Fig. 1c), a pure phased lineshape can be obtained when the delay after p_2 is longer than T_2^*. In this case, p_3 is a selective 180° pulse.

CONCLUSIONS

Complete cancellation of the large first-order quadrupolar interaction imposes high demands on the experimental setup and optimization of the STMAS experiment. The described procedure calibrates the magic angle, t_1 initial evolution time, excitation, and conversion pulses that are critical to the STMAS experiment.

Magic angle setting and spinning speed stability are the two most important factors to the STMAS experiment. The described procedure is capable of calibrating the magic angle within a few thousands of a degree and most modern NMR consoles and MAS probes can meet the 10^{-4} demand on spinning speed stability. Reproducing the magic angle for sample change requires mechanical stability of the probe mount. The MAS probe used in this work is equipped with a sample changer line from the top of the magnet and shows very little change on the magic angle setting after sample changes. In case of probes that must be taken out of magnets to change samples, improved design on probe stator positioning is probably required. The procedure here uses samples with good spectral sensitivities. Optimized parameters using the setup samples can be applied to samples of interests likely having low sensitivities. After solving the practical issues of STMAS, one may take full advantage of high efficiencies of the single-quantum experiment for high-resolution solid state NMR of quadrupolar nuclei.

ACKNOWLEDGMENTS

This work is supported by the National High Magnetic Field Laboratory through National Science Foundation Cooperative Agreement DMR-0084173 and by CNRS and University Louis Pasteur, Strasbourg France. Dr. F. Engelke from Bruker Rheinstetten, Germany, is thanked for triggering and managing improvements of MAS probes for easier mechanical setting of the magic angle.

REFERENCES

1. Z. Gan, Isotropic NMR spectra of half-integer quadrupolar nuclei using satellite transitions and magic angle spinning, *J. Am. Chem. Soc.* **122,** 3242 (2000).
2. Z. Gan, Satellite transition magic angle spinning nuclear magnetic resonance spectroscopy of half-integer quadrupolar nuclei, *J. Chem. Phys.* **114,** 10845 (2001).
3. "Encyclopedia of Materials Science & Technology," Elsevier, Amsterdam (2001). Also available at http://www.elsevier.com/locate/emsat.
4. L. Frydman, "MQMAS Fundamentals," NMR Encyclopedia, 2nd ed., Wiley, New York (2001).
5. A. Medek, J. S. Harwood, and L. Frydman, Multiple-quantum magic angle spinning NMR: A new method for the study of quadrupolar nuclei in solids, *J. Am. Chem. Soc.* **117,** 12779 (1995).
6. J.-P. Amoureux, C. Fernandez, and S. Steuernagel, Z filtering in MQMAS NMR, *J. Magn. Reson.* **123,** 116 (1996).
7. K. J. Pike, S. E. Ashbrook, and S. Wimperis, Two-dimensional satellite-transition MAS NMR of quadrupolar nuclei: Shifted echoes, high-spin nuclei and resolution, *Chem. Phys. Lett.* **345,** 400 (2001).
8. D. Massiot, B. Touzo, D. Trumeau, J. P. Coutures, J. Virlet, P. Florian, and P. J. Grandinetti, Two-dimensional magic angle spinning isotropic reconstruction sequences for quadrupolar nuclei, *Solid State NMR* **6,** 73 (1996).
9. J.-P. Amoureux, "MQMAS," NMR Encyclopedia, 2nd ed., Wiley, New York (2001).
10. S. P. Brown, S. J. Heyes, and S. Wimperis, Two-dimensional MAS multiple-quantum NMR of quadrupolar nuclei: Removal of inhomogeneous second-order broadening, *J. Magn. Reson.* **119,** 280 (1996).
11. D. Fenzke, D. Freude, T. Froehlich, and J. Haase, NMR intensity measurements of half-integer quadrupole nuclei, *Chem. Phys. Lett.* **111,** 171 (1984).
12. M. E. Smith and E. R. H. Van Eck, Recent advances in experimental solid state NMR methodology for half-integer spin quadrupolar nuclei, *Prog. Nucl. Magn. Reson. Spectrosc.* **34,** 159 (1999).
13. F. Taulelle, NMR of quadrupolar nuclei in the solid state, *NATO ASI Ser. C* **322,** 393 (1990).
14. C. Jaeger, How to get more from aluminum-27 MAS NMR by high-speed satellite-transition spectroscopy, *J. Magn. Reson.* **99,** 353 (1992).
15. C. Jaeger, J. Rocha, and J. Klinowski, High-speed satellite transition aluminum-27 MAS NMR spectroscopy, *Chem. Phys. Lett.* **188,** 208 (1992).
16. H. J. Jakobsen, J. Skibsted, H. Bildsoee, and N. C. Nielsen, Magic angle spinning NMR spectra of satellite transitions for quadrupolar nuclei in solids, *J. Magn. Reson.* **85,** 173 (1989).
17. J. S. Frye and G. E. Maciel, Setting the magic angle using a quadrupolar nuclide, *J. Magn. Reson.* **48,** 125 (1982).
18. L. B. Alemany, D. Massiot, B. L. Sherriff, M. E. Smith, and F. Taulelle, Observation and accurate quantification of aluminum-27 MAS NMR spectra of some aluminum silicon oxide (Al_2SiO_5) polymorphs containing sites with large quadrupole interactions, *Chem. Phys. Lett.* **177,** 301 (1991).
19. A. Samoson, Satellite transition high-resolution NMR of quadrupolar nuclei in powders, *Chem. Phys. Lett.* **119,** 29 (1985).